Computation of Radial Electric Field in the Turbulent Edge Plasma of the T-10 Tokamak

R.V. Shurygin 1), A.V. Melnikov 1), A.A. Mavrin 1)

1) Nuclear Fusion Institute, RRC "Kurchatov Institute", Moscow, Russia

e-mail contact of main author: regulxx@rambler.ru

Abstract. Numerical computation of turbulent dynamics of edge plasma was carried out. The computation is based on the solution of nonlinear MHD equations in the frame of reduced two -fluid Braginskii's hydrodynamics. It is shown that under transition from OH to ECRH regime, the driving force of turbulence linked with magnetic curvature increases. The Reynolds turbulent force also increases. The growth of this force leads to the generation of higher poloidal velocity. Since this velocity is negative and directed as the diamagnetic drift of ions, then, in accordance with the equation for radial force balance of ions, the value of radial electric field decreases. Computations qualitatively confirm the experiment al results obtained in T-10 tokamak.

1. Introduction

It is widely recognized that the radial electric field E_r plays an important role in plasma confinement via [$E_r \times B_{tor}$] shearing stabilization. Theoretical description of the E_r formation, based on turbulent dynamics and, specifically, the numerical modeling of the edge plasma electrostatic potential in the T-10 tokamak is the topic of this paper.

Direct measurements by the Heavy Ion Beam Probe (HIBP) diagnostic have shown that electrostatic potential forms the negative well ($E_r = -\partial\Phi/\partial r < 0$) in Ohmic and ECRH regimes with moderate densities ($n_e = 1.5 - 2.5\times10^{19}$ m^{-3}) in the T-10 tokamak [1, 2]. Transition from OH to ECRH regime was accompanied by the decrease of the absolute potential value, i.e. the module of radial electric field decreased, $|E_r|^{ECRH} < |E_r|^{OH}$, while its sign still remains negative. Main goal of the paper is calculations of the radial profile of electrostatic potential in the turbulent scrap-off layer (SOL) plasma of the T-10 tokamak for two abovementioned regimes.

2. Basic equations

We use the set of reduced two-fluid Braginskii equations presented in [3-7]. Assuming that the longitudinal ion velocity is zero, $u_{\|}=0$, and ignoring the thermal current, we can obtain the following set of four-field $\{\phi, n, p_e, p_i\}$ nonlinear MHD equations describing the behavior of the collisional plasma in the slab SOL of tokamak:

$$\frac{\partial W}{\partial t} + \mathbf{V}_E \cdot \nabla W + H_{NL} = \frac{B\omega_{ci}}{c}\nabla_{\|} J_{\|} - \omega_{ci}\frac{2\nabla B}{B}\cdot\mathbf{b}\times\nabla(p_e + p_i) + \mu_{\perp}\Delta_{\perp} W \quad (1)$$

$$\frac{\partial n}{\partial t} + \mathbf{V}_E \cdot \nabla n = \frac{\nabla_{\|} J_{\|}}{e} + \mathbf{Q}\cdot(\nabla p_e - en\nabla\phi) + D_{\perp}\Delta_{\perp} n \quad (2)$$

$$\frac{3}{2}\left(\frac{\partial p_e}{\partial t} + \mathbf{V}_E \cdot \nabla p_e\right) = \frac{5p_e\nabla_{\|} J_{\|}}{2en} - \frac{5}{2}\mathbf{Q}\cdot[p_e(e\nabla\phi) - \nabla(p_e T_e)] - W_{ei} - \nabla(\mathbf{q}_{e\perp} + \mathbf{q}_{e\|}) \quad (3)$$

$$\frac{3}{2}\left(\frac{\partial p_i}{\partial t} + \mathbf{V}_E \cdot \nabla p_i\right) = \frac{5p_i\nabla_{\|} J_{\|}}{2en} - \frac{5}{2}\mathbf{Q}\cdot[p_i(e\nabla\phi - \frac{\nabla(p_e + p_i)}{n}) + \nabla(p_i T_i)] + W_{ei} - \nabla(\mathbf{q}_{i\perp} + \mathbf{q}_{e\|}) \quad (4)$$

$$\eta_0 J_\parallel = - \nabla_\parallel \phi + \frac{\nabla_\parallel p_e}{en}, \tag{5}$$

$$W = \nabla_\perp (en\nabla_\perp \phi + \nabla_\perp p_i), \quad \mathbf{Q} = \frac{2c}{e} \frac{\mathbf{b}\times\nabla B}{B}. \tag{6}$$

$W_{ei} = 3\frac{m_e}{M_i}\nu_{ei}(p_e - p_i)$ is the exchange term, ν_{ei} is the electron–ion collision frequency.

The function H_{NL} contains the nonlinear terms that arise during, when reducing the ion momentum equation in order to derive an equation for a vortex. As it was shown in [3,7], this function could be represented as:

$$H_{NL} = \frac{1}{2}\left\{en\mathbf{V}_{pi}\cdot\nabla(\nabla_\perp^2\phi) - m\omega_{ci}\mathbf{b}\times\nabla n\cdot\nabla V_E^2\right\} - \frac{1}{2}\left\{\mathbf{V}_E\cdot\nabla(\nabla_\perp^2 p_i) - \nabla_\perp^2(\mathbf{V}_E\nabla p_i)\right\}. \tag{7}$$

In deriving Eqs. (1)–(6) it was assumed that the magnetic field in the Cartesian coordinates (x, y, z) has the form:

$$\mathbf{B} = B_0(1 - \frac{x}{R_0})[\mathbf{e_z} + \frac{\varepsilon}{q}\mathbf{e_y}]. \tag{8}$$

Here, **B** is the equilibrium tokamak magnetic field; q is the safety factor, $\varepsilon = r/R_0$, r and R_0 are the minor and major radii of a tokamak, respectively. In Eqs. (1) –(6), the plasma density is $n(x, y, t)$, the electron and ion pressures are $p_{e,i}(x, y, t)$; the electrostatic potential $\phi(x, y, t)$ describes the oscillations of the electric field, and the rest of the notations are as follows:

$$\mathbf{V}_E = \frac{c[\mathbf{B}\times\nabla\phi]}{B^2}, \quad \Delta_\perp = \frac{\partial^2}{\partial x^2} + \frac{\partial^2}{\partial y^2}, \quad \nabla_\parallel = \vec{b}\cdot\nabla = \frac{\mathbf{B}}{B}\cdot\nabla.$$

It is convenient to present Eqs. (1)–(6) in dimensionless form using the new variables:

$$t \to t/t_*, \quad (x, y) \to (x/d, y/d), \quad \phi \to e\phi/T_*,$$
$$n \to n/n_*, \quad p_{e,i} \to p_{e,i}/p_*, \quad k_y \to k_y \cdot d, \quad \rho = \rho_s/d, \quad \omega_0 = \rho^2\omega_{ci},$$

where $t_* = \frac{1}{\omega_0}$, $\rho_S = \frac{V_*}{\omega_{ci}}$, $V_* = \sqrt{\frac{T_*}{m_i}}$, $\omega_{ce,i} = \frac{eB}{m_{e,i}c}$, $\eta = \frac{m_e\nu_{ei}}{2e^2N_0}$, $p_* = n_*T_*$, $x = (r-r_0)$, $d = a-r_0$ is the width of the computation slab, r_0 – is a radius of its inner boundary. The normalized values for density and electron temperature were taken to be $n_* = 10^{19}$ m^{-3} and $T_* = 350$ eV. Also we use dimensionless radial variable $0 < x = (r-r_0)/(a-r_0) < 1$.

In terms of these new variables, Eqs. (1)–(6) can be converted to the form [4]:

$$\frac{DW}{Dt} + H_{NL} = \nabla_\parallel J - g_B\frac{\partial p}{\partial y} + \nu_\perp\cdot\Delta_\perp W, \tag{9}$$

$$\frac{Dn}{Dt} = \nabla_\parallel J + g_B\frac{\partial(N_0\phi - p_e)}{\partial y} + D_\perp\cdot\Delta_\perp n, \tag{10}$$

$$\frac{3}{2}\frac{Dp_e}{Dt} = \frac{5}{2}T_{e0}\nabla_\parallel J + \frac{5}{2}g_B K_e - w_{ei} + \chi_{\parallel e}\nabla_\parallel^2 p_e + \chi_{\perp e}\cdot\nabla_\perp^2 p_e, \tag{11}$$

$$\frac{3}{2}\frac{Dp_i}{Dt} = \frac{5}{2}T_{i0}\nabla_{\|}J \quad + \frac{5}{2}g_B K_i + w_{ei} + \chi_{\|i}\nabla_{\|}^2 p_i + \chi_{\perp i}\cdot\nabla_{\perp}^2 p_i, \tag{12}$$

$$\eta_0 J = -\nabla_{\|}(\phi - p_e/N_0), \tag{13}$$

$$K_e = p_{e0}\frac{\partial\phi}{\partial y} - 2T_{e0}\frac{\partial p_e}{\partial y} + T_{e0}{}^2\frac{\partial n}{\partial y}, \qquad K_i = p_{i0}\frac{\partial\phi}{\partial y} + T_{i0}\frac{\partial(p_i - p_e)}{\partial y} - T_{i0}{}^2\frac{\partial n}{\partial y},$$

$$W = \rho^2\cdot\nabla_{\perp}(n\nabla_{\perp}\phi + \nabla_{\perp}p_i), \qquad p = p_e + p_i. \tag{14}$$

Here

$$\frac{D}{Dt} = \frac{\partial}{\partial t} + \{\phi, \ \}, \qquad \{A,B\} = \mathbf{e}_z\nabla A\times\nabla B,$$

$$g_B = \frac{2d}{R_0}, \quad \eta_0 = \frac{\nu_{ei}}{\omega_{ce}}, \quad \chi_{\|e} = \frac{3.16\omega_{ce}}{\nu_{ei}}, \quad \chi_{\|i} = \frac{3.9\omega_{ci}}{\nu_{ii}}, \quad w_{ei} = 3\frac{m_e}{M_i}\frac{\nu_{ei}}{\omega_0}(p_e - p_i),$$

N_0 is the amplitude of the zeroth harmonic of the density.

Note that apart from the electric drift, we take into account the ion diamagnetic drift, as well as density fluctuation in the equation for the vorticity. It leads to the appearance additional nonlinear terms H_{NL}:

$$H_{NL} = \frac{\rho^2}{2}\left[\nabla_{\perp}^2\{\phi, p_i\} - \{\phi, \nabla_{\perp}^2 p_i\} + \{p_i, \nabla_{\perp}^2\phi\} + \{V_E^2, n\}\right]. \tag{15}$$

3. Method of solution

For numerical solution of basic set of equations we use a quasi -spectral approach based on the Galerkin method. All functions $f=\{n, \phi, p_e, p_i\}$ are chosen as the sum of helical waves with the same helicity, i.e.

$$f(x,y,z,t) = \sum f_{ky,kz}\exp[i(k_y y - k_z z)] = \sum f_{ky}\exp[ik_y(y-\alpha z)], \tag{16}$$

where $\alpha=k_z/k_y=const$. For modes with $k_z=n/R$ and $k_y=m/r$ in a toroidal geometry we have $\alpha=\varepsilon/q_{res}$, $\varepsilon=r_{res}/R$. It is well known that this approach reduces the problem of solving 3D equations to that of solving 2D equations. We switch to the new helical variable $Y \to y-\alpha z$ and assume that the following Fourier series expansion is valid for each of the above functions f:

$$f(x,Y,t) = f_0(x,t) + \sum_{L=1}^{L_{MAX}}\left[f_{sL}\sin(mk_{oy}Y) + f_{cL}\cos(mk_{oy}Y)\right], \ m = m(L), \ k_{0y} = d/r_{res}. \tag{17}$$

The quantity q_{res} is assumed to be only integer, and the integer mode numbers $m = m(L)$ and $n = n(L)$ are chosen such that $m(L)/n(L) = q_{res}$.

Substituting expansion (17) into Eqs. (1)–(6), we obtain a set of equations for the poloidal harmonics $\{f_{SL}, f_{CL}\}$. In symbolic form, this set of $2L_{\mathrm{MAX}}$ equations can be written as:

$$\frac{\partial\mathbf{f}_{S,CL}}{\partial t} = \hat{L}_L(\mathbf{f}_{S,CL}) + \hat{D}_L(\mathbf{f}_{S,CL}) + \hat{N}_L(\mathbf{f}_{S,CL}), \quad L = 1,2....L_{MAX}. \tag{18}$$

In numerical simulations we use the following simple two -level predictor–corrector scheme:

$$\frac{X_i^{n+1/2} - X_i^n}{\tau/2} = \hat{L}(X_i^{n+1/2}) + \hat{D}(X_{i-1}^{n+1/2}, X_i^{n+1/2}, X_{i+1}^{n+1/2}) + N(X_i^n)$$
$$\frac{X_i^{n+1} - X_i^n}{\tau} = \hat{L}(X_i^{n+1}) + \hat{D}(X_{i-1}^{n+1}, X_i^{n+1}, X_{i+1}^{n+1}) + N(X_i^{n+1/2}),$$

where $\hat{L}$, $\hat{D}$ and $\hat{N}$ are the linear, diffusion and nonlinear operators in Eqs. (9)–(14). At each time step, the difference equations were solved by the matrix sweep method.

The equations for the zeroth harmonics (the background quantities) $f_0=\{N_0, U_{0y}, P_{e0}, P_{i0}\}$ can easily be obtained by averaging Eqs. (9)–(12) over the angle Y and by supplementing the right-hand sides of the resulting equations with the source terms S_N, S_{pe}, and S_{pi}:

$$\frac{\partial N_0}{\partial t} + \frac{\partial \Gamma}{\partial x} = D_0 \frac{\partial^2 N_0}{\partial x^2} + S_N \tag{19}$$
$$\frac{\partial P_{e0}}{\partial t} + \frac{\partial Q_e}{\partial x} = \chi_{e0} \frac{\partial^2 P_{e0}}{\partial x^2} - w_{ei} + S_{pe} \tag{20}$$
$$\frac{\partial P_{i0}}{\partial t} + \frac{\partial Q_i}{\partial x} = \chi_{i0} \frac{\partial^2 P_{i0}}{\partial x^2} + w_{ei} + S_{pi} \tag{21}$$

In Eqs. (19)–(21), the turbulent fluxes are described by the following expressions: the particle fluxes are $\Gamma = \langle n \cdot V_{Ex} \rangle_Y$, the electron and ion heat fluxes are $Q_\alpha = \langle p_\alpha \cdot V_{Ex} \rangle_Y$ $\alpha = e, i$, the angle brackets denote averaging over the periodic coordinate Y: $\langle f \rangle_Y = \frac{1}{L_Y} \int_0^{L_Y} f(Y) dY$, $L_Y=2\pi/k_{0y}$.

Averaging of vorticity equation (9) finally gives us the following dimensionless equation for the evolution of poloidal momentum $G_{0y}=N_0U_{0y}$ [4]:

$$\frac{\partial G_{0y}}{\partial t} + \frac{\partial R}{\partial x} = \nu_0 \frac{\partial^2 G_{0y}}{\partial x^2} - \frac{(\nu_{neo} + \nu_{cx})}{\omega_0} (G_{0y} - G_{neo}), \tag{22}$$

where $R = \rho < V_{Ex} (N_0 V_{Ey} + \frac{dp_i}{dx}) > -V_E \Gamma$ is the turbulent Reynolds stress.

Note that taking into account new nonlinear terms H_{NL} in the vorticity equation (9) results in the appearance of additional term $<V_{Ex} \cdot dp_i/dx>$ in the turbulent Reynolds stress tensor, which plays an important role in numerical computation.

Equation for the electric field follows from the ion radial force balance:

$$V_E = -U_{0y} + V_{pi}, \qquad V_{pi} = \frac{\rho}{N_0} \frac{dp_i}{dx} < 0, \qquad V_E = \frac{cE}{BV_*}. \tag{23}$$

$$\phi(x) = \int_x^1 E(x) dx, \quad \phi(1) = 0$$

Under the assumption that the waves are of the same helicity, we can use the expansion $k_z/k_y = \varepsilon/q(x_{res})$ at the resonant point to obtain the following representation for $\nabla_\parallel f$ in a thin slab layer:

$$\nabla_{\|} f = \frac{\varepsilon}{q(x)}\frac{\partial f}{\partial y} + \frac{\partial f}{\partial z} \approx -\frac{d}{L_S}(x - x_{res})\frac{\partial f}{\partial Y}, \quad L_S = \frac{qR_0}{(1-s)}, \quad s = \frac{rq'}{q}. \tag{24}$$

Numerical simulations were carried out for the edge region, r_0 = 26 cm < r < 30 cm=a, of T-10 for the following parameters: R = 150 cm, a = 30 cm, d = 4 cm, B = 2.31 T, q_{res} = 3, $N_0(r_0)$ = 1.6×10^{19} m^{-3}, $N_0(a)$ = 0.2×10^{19} m^{-3}, $T_i(r_0)$ = 80 eV, $T_i(a)$ = 12 eV. The choice of the resonant helical modes is obeyed to the rule: $m = 3\cdot k$, k=1, 2, .., K_{max}; K_{max} = < 30. The radial extent of the calculation layer was limited due to the single helicity approach. Increase of electron temperature $T_e(r_0)$ on the inner boundary of the calculation layer was used to simulate transition from OH to ECRH regime with various level of input EC-power.

4. Calculation of radial electric field

Numerical results show the negative electric potential in the OH regime, $T_e(r_0)^{OH}$ = 60 eV. The gradual increase of the boundary electron temperature $T_e(r_0)^{ECRH}$ = 90, 120, 150 eV leads to corresponding decrease of the absolute value of the electric potential, as shown in Fig. 1. Poloidal velocity U_{0y} is shown in Fig. 2. The value of electric potential and mean E_r shows qualitative agreement with experimental data obtained both in Ohmic and ECR heating regimes [8-10]. Dependence of E_r averaged over the calculation layer on the boundary electron temperature $T_e(r_0)$ is shown in Fig. 3. The transition from low $T_e(r_0)$ (OH) to higher $T_e(r_0)$ (ECRH) results in decrease of the absolute value of electric field $|E_r|^{ECRH} < |E_r|^{OH}$, remaining its negative sign.

Numerical calculations shows, that with growth of electron temperature under transition from OH to ECRH regime there is an increase of amplitudes of fluctuations of potential because of increase of the driving force of turbulence linked with magnetic curvature (a member $\sim g_B\partial(p_i+p_e)/\partial y$ in the equation (9)). Thus Reynolds's turbulent force increases (see a Fig. 4). The growth of this force leads to the additional generation of poloidal velocity. Since this velocity is negative $U_{0y} < 0$ and directed as the diamagnetic drift of ions $V_{pi} < 0$, then, in accordance with the equation for radial force balance of ions (23), the value of radial electric field decreases with growth $|U_{oy}|$, see Fig. 3. Thus, the computation results qualitatively agree with experimental data.

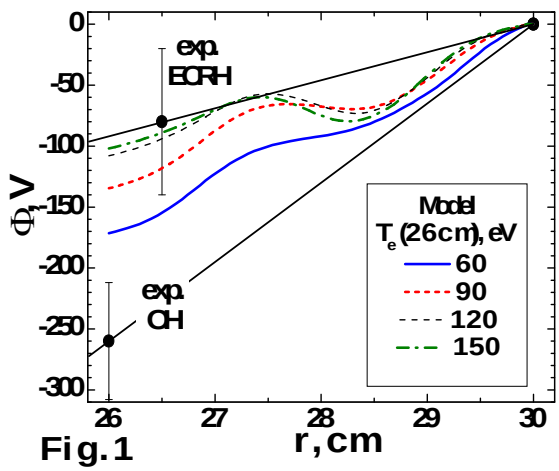

Fig. 1

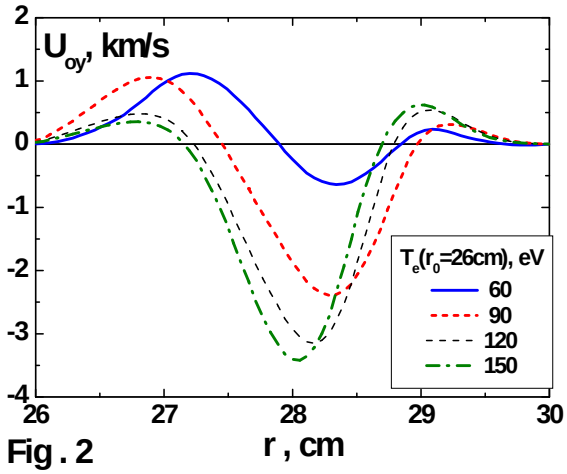

Fig. 2

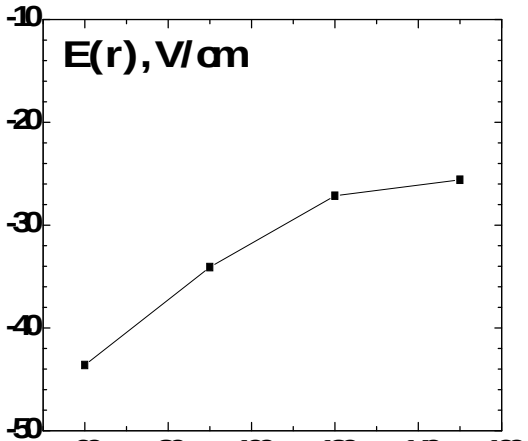

Fig. 3

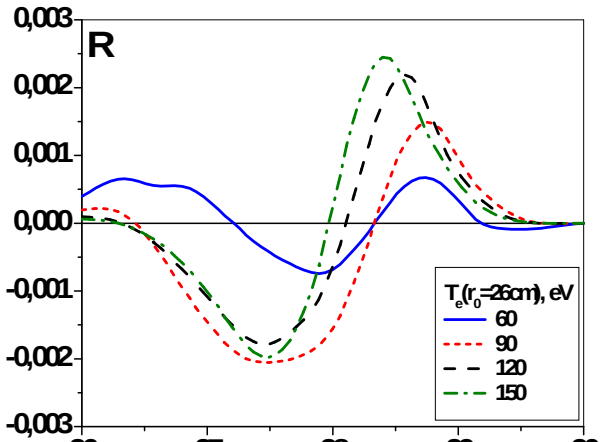

Fig. 4

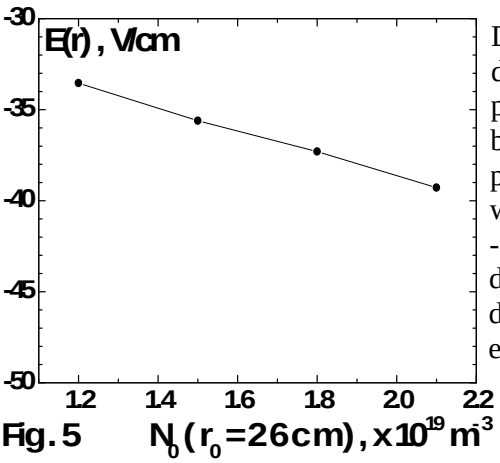

Fig. 5

Dependence of mean electric field on the plasma density was also modelled for the same plasma parameters. The plasma density at the inner boundary was chosen to be the only varied parameter for numerical simulations. Calculations were performed for the realistic values of $N_0(r_0)$ =1.2 - 2.1×10^{19} m^{-3}. Figure 5 shows the inverse dependence of modeled electric field on the plasma density, which agrees with the tendency, observed experimentally in T-10 [2].

5. Conclusions

The model for the E_r calculation based on the Braginskii's hydrodynamics was developed for the periphery of the tokamak plasma. Numerical results for T-10 conditions show qualitative agreement with direct experimental data, obtained by HIBP. Moreover, the experimental dependences of E_r on plasma temperature and density were obtained by modeling. So, E_r in the strong turbulent plasma of the tokamak periphery was satisfactory described by d eveloped model.

Acknowledgments

This work was supported by Grants RFBR 08-02-01326, 07-02-01001 and INTAS 100008-8046.

References

[1] MELNIKOV, A.V., et al., "Study of the core plasma potential and turbulence evolution during ECRH in the T-10 tokamak", 32-nd EPS Conf. on Plasma Phys. Tarragona, 2005, P-4.052.

[2] MELNIKOV, A.V., et al., "Investigation of the plasma potential behaviour at the periphery of the T-10 tokamak", 33-nd EPS Conf. on Plasma Phys., Rome, 2006, P-4.089.

[3] XU X.Q., et al., "Low-to-high confinement transition simulations in divertor geometry", Phys. Plasmas **7** (2000) 1951.

[4] SHURYGIN, R.V. "Resistive Drift–Alfvén Turbulence in a Tokamak Edge Plasma", Plasma Phys, Reports **32** (2006) 799

[5] SCOTT, B.D., "Three-dimensional computation of drift Alfvén turbulence", Plasma Phys. and Control. Fusion **39** (1997) 1635.

[6] ZEILER, A., DRAKE, J.F., ROGERS, B., " Nonlinear reduced Braginskii equations with ion thermal dynamics in toroidal plasma", Phys. Plasmas **4** (1997) 2134.

[7] SIMAKOV, A.N., CATTO, P.J., "Drift-ordered fluid equations for field-aligned modes in low-β collisional plasma with equilibrium pressure pedestals", Phys. Plasmas **10** (2003) 4744.

[8] PERFILOV, S.V., et al., 34-th EPS Conf. on Plasma Physics, Warsaw, ECA, vol.31F, P-2.058 (2007).

[9] SHURYGIN, R.V. MELNIKOV, A.V., et al., Plasma Phys, Reports submitted (2008).